Analysis of Event-Related fMRI Data Using Best Clustering Bases

François G. Meyer and Jatuporn Chinrungrueng

Department of Electrical Engineering,
University of Colorado at Boulder, Boulder CO, 80309-0425
francois.meyer@colorado.edu
http://ece-www.colorado.edu/~fmeyer

Abstract. We explore a new paradigm for the analysis of event-related functional magnetic resonance images (fMRI) of brain activity. We regard the fMRI data as a very large set of time series $x_i(t)$, indexed by the position i of a voxel inside the brain. The decision that a voxel i_0 is activated is based not solely on the value of the fMRI signal at i_0, but rather on the comparison of all time series $x_i(t)$ in a small neighborhood W_{i_0} around i_0. We construct basis functions on which the projection of the fMRI data reveals the organization of the time-series $x_i(t)$ into "activated", and "non-activated" clusters. These "clustering basis functions" are selected from large libraries of wavelet packets according to their ability to separate the fMRI time-series into the activated cluster and a non activated cluster. This principle exploits the intrinsic spatial correlation that is present in the data.

1 Introduction

Functional Magnetic Resonance Imaging (fMRI), utilizes the fact that oxygenated blood and deoxygenated blood have different magnetic susceptibility to create maps of changes in cerebral venous oxygen concentration that correlate with neuronal activity. There are currently two types of experimental designs: the periodic stimulus design (block design) and the event-related stimulus design (odd-ball design). The detection of activation using event-related fMRI data is the more difficult problem and will be the focus of this work. The analysis of event-related fMRI data commonly relies on the assumption that the fMRI signal $\mathbf{x}_i = [x_i(0), \cdots, x_i(T-1)]^t$ at a voxel i inside the brain is obtained by convolving the stimulus waveform $\mathbf{s}_i = [s_i(0), \cdots, s_i(T-1)]^t$ with some unknown hemodynamic response function $\mathbf{h}_i$ [1]. Unfortunately, it has become clear that there is a nonlinear relationship between the variation in the fMRI signal and the stimulus presentation [2]. In the absence of any detailed substantive understanding of the mechanism of the fMRI response, we advocate a non parametric data-driven approach that can better account for all important features present in the data. Fig. 1 shows a block diagram that illustrates the principle of our approach. We consider a group of voxels, and the corresponding time series, from a small window W_{i_0} inside the brain. We partition these time series into two

clusters. If W_{i_0} is located in a part of the brain that is activated, then one of the two clusters encompasses the activated voxels, or activated time series.
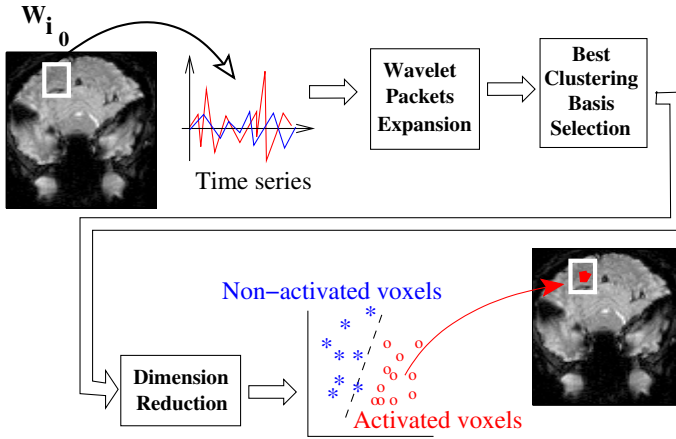

Fig. 1. We partition the time series inside a small window W_{i_0} into two clusters. The clustering is performed on the wavelet packet coefficients (feature space)

The other cluster contains time series that correspond to background activity. If the window is in a part of the brain with no activity correlated to the stimulus, then all time series are considered to be background activity. As W_{i_0} is moved throughout the brain, local decision (activation/non activation) are computed for each voxel $i \in W_{i_0}$. This principle exploits the intrinsic spatial correlation that is present in the data. Indeed, truly activated voxels tend to be spatially clustered, while falsely activated voxels will tend to be scattered. One can then increase the sensitivity of the detection by using the fact that real activation should be more clustered than artifactual activation caused by noise. These local decisions are combined to generate a more robust global activation score, which can be presented in the form of an activation map. Unlike global clustering methods [3], our local clustering approach only partitions the time series in a small region of the brain. Furthermore, the clustering of the time series is not performed directly on the raw fMRI signal. Instead, the raw data are projected on a set of basis functions conveniently chosen for their discriminating power, and their robustness to noise. If the stimulus is periodic, the Fourier basis provide the most interesting projection of the data [4]. If the stimulus is not periodic, then we need to replace the Fourier transform with a transform that can efficiently represent the nonlinear and non-stationary structures present in event-related data. Several studies indicate that one finds dynamic changes of the fMRI signal in time, frequency, and in space [5, 6]. Wavelet packets are time-frequency "atoms" that are localized in time and in frequency. Wavelet packets have been used quite successfully to analyze transients in evoked poten-

tials or electroencephalograms [7]. We favor therefore the use of wavelet packets to perform the analysis of the event-related hemodynamic response $\mathbf{x}_i$. Instead of using a fixed basis we will select a basis among a very large and highly redundant dictionary of wavelet packets, $\mathcal{B} = \{\boldsymbol{\psi}_\gamma\}$. Because the dictionary is highly redundant, one can select those wavelet packets $\boldsymbol{\psi}_\gamma = [\psi_\gamma(0), \cdots, \psi_\gamma(T-1)]^t$ (where γ is a parameter indexing the functions) on which the projection of event-related fMRI data reveals the organization of the time-series into "activated", and "non-activated" clusters. The representation of an event-related signal $\mathbf{x}_i$ in such a basis is defined by $\mathbf{x}_i = \sum_\gamma \alpha_\gamma(\mathbf{x}_i)\boldsymbol{\psi}_\gamma$. This approach does not assume any particular model of the hemodynamic response, but rather tries to "let the data speak for themselves". The paper is organized as follows. In Section 2 we provide a brief review of the wavelet packets and the best-basis algorithm [8]. In Section 3 we describe the new best clustering basis algorithm. Results of experiments conducted on synthetic and *in-vivo* fMRI data are presented in Section 4. Finally, a conclusion and a discussion can be found in Section 5.
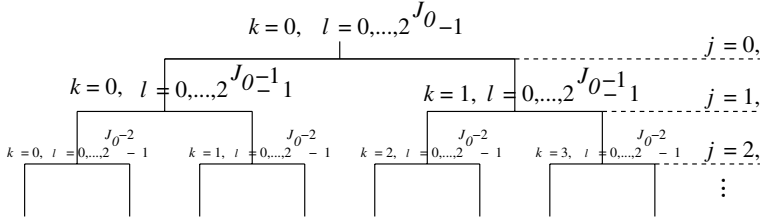

Fig. 2. Wavelet packets tree shows the index $\gamma = (j, k, l)$ at each node.

2   Wavelet Packets, Best-Basis

Let $\psi^0(t)$ be the scaling function and let $\psi^1(t)$ be the wavelet associated with a multiresolution analysis [9]. Let $\{h_n\}$ be the lowpass filter, and let $\{g_n\}$ be the high pass filter associated with this wavelet transform. The basic wavelet packets are given by

$$\psi^{2n}(t) = \sum_k h_k\, \psi^n(2t - k) \quad , \qquad \psi^{2n+1}(t) = \sum_k g_k\, \psi^n(2t - k). \qquad (1)$$

A multiscale wavelet packet is defined by $\psi_{j,k,l}(t) = \psi^k(2^j t - l)$. The index $\gamma = (j, k, l)$ can be interpreted as follows :

- $j = 0, \ldots, \mathrm{J} \le J_0$ is the scale : $\psi_{j,k,l}$ has a support of size 2^{-j}.
- $k = 0, \ldots, 2^j - 1$ is the frequency index at a given scale j : $\psi_{j,k,l}$ has roughly k oscillations.
- $l = 0, \ldots, 2^{J_0-j} - 1$ is the translation index within a node (j, k) : $\psi_{j,k,l}$ is located at $l\, 2^{-j}$.

As shown in Fig. 2 the library of wavelet packets organizes itself into a binary tree, where the nodes of the tree represent subspaces with different time-frequency localization characteristics. The $2^{J_0} \times 1$ discrete wavelet packet basis vector $\boldsymbol{\psi}_{j,k,l}$ is sometimes written as $\boldsymbol{\psi}_\gamma$. We define the $2^{J_0} \times 2^{J_0-j}$ matrix

$$\boldsymbol{\Psi}_{j,k} = \left[\boldsymbol{\psi}_{j,k,0} | \cdots | \boldsymbol{\psi}_{j,k,2^{J_0-j}-1} \right] \tag{2}$$

to be the collection of wavelet packets at node (j,k) stacked together. The wavelet packet coefficients $\alpha_{j,k,l}, \; l = 0, \cdots, 2^{J_0-j}$ of the vector $\mathbf{x}$ at the node (j,k) are given by the projections of $\mathbf{x}$ on the 2^{J_0-j} wavelet packets stacked inside the matrix $\boldsymbol{\Psi}_{j,k}$,

$$\left[\alpha_{j,k,0} \cdots \alpha_{j,k,2^{J_0-j}-1} \right]^t = \boldsymbol{\Psi}_{j,k}^t \mathbf{x}. \tag{3}$$

Let us associate the dyadic frequency interval $[2^j k, 2^j(k+1))$ to the wavelet packet node $\boldsymbol{\Psi}_{j,k}$. If a collection of intervals $[2^j k, 2^j(k+1))$ provides a cover of the time-frequency plane, then the corresponding set of $\boldsymbol{\Psi}_{j,k}$ forms an orthonormal basis [8]. If we perform a dyadic subdivision at each level, we get 2^{2^J} bases for J levels. Clearly, we have an extremely large amount of freedom for the construction of orthogonal bases from the wavelet packet library $\{\psi_{j,k,l}\}$. This greater flexibility can be exploited to increase the efficiency of the representation. Coifman and Wickerhauser [8] suggested to use a dynamic programming algorithm with order $T \log(T)$ to search for that *best basis* which is optimal according to a given cost function $\mathcal{M}$. These dictionaries have been used recently in the context of supervised classification [10]. In this work we intend to address a more general and deeper problem, where one wants to determine the best clustering basis without having access to a training set containing activated and non activated signals.

3   Best Clustering Bases

In our problem we need a cost functional $\mathcal{M}$ that measures how well a basis function ψ_γ can partition a set of signals into meaningful clusters. We illustrate our idea with a simple geometric example shown in Fig. 3. We consider two sets of points distributed respectively inside the two circles A and B (see Fig. 3). We consider two different bases: $(\mathbf{a}_1, \mathbf{a}_2)$, and $(\mathbf{b}_1, \mathbf{b}_2)$. One could imagine that the bases $(\mathbf{a1}, \mathbf{a2})$ and $(\mathbf{b1}, \mathbf{b2})$ correspond to two different wavelet packet bases. In order to discover the two clusters A and B, we can partition the points using a clustering algorithm. We can use either one of the two bases to perform the clustering. However, to simplify the clustering process and to avoid the curse of dimensionality, one should use the basis that concentrates its discriminatory power onto a small number of basis functions. Let us consider a vector $\mathbf{v}$, and let us project the dataset on this vector. If we cluster the projections into two partitions, we can define the discriminatory power of $\mathbf{v}$ as the distance between the two centroids. according to this definition, the vectors $\mathbf{a}_1$ and $\mathbf{a}_2$ have the same discriminatory power δ (see Fig. 3). However,
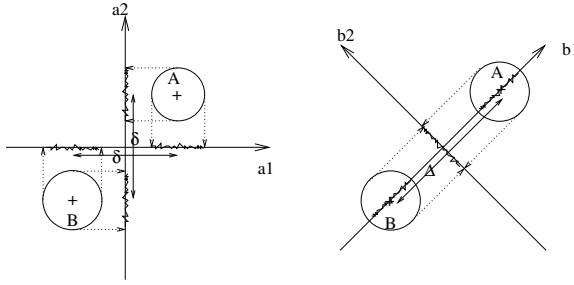
Fig. 3. The basis $(\mathbf{b}_1, \mathbf{b}_2)$ concentrates its discriminatory power on a single vector $\mathbf{b}_1$, whereas the basis $(\mathbf{a}_1, \mathbf{a}_2)$ distributes the power equally on the vectors $\mathbf{a}_1$ and $\mathbf{a}_2$.

the vector $\mathbf{b}_1$ has a discriminatory power Δ, that is larger than δ. The vector $\mathbf{b}_2$ on the other hand does not discriminate one cluster from another. Therefore, if we use the basis $(\mathbf{b}_1, \mathbf{b}_2)$ the discriminatory power is only concentrated on the vector $\mathbf{b}_1$. We should choose the basis $(\mathbf{b}_1, \mathbf{b}_2)$ and perform the clustering using only the vector $\mathbf{b}_1$. Our clustering cost functional reflects this principle and selects the basis that concentrates most discriminatory power on a small number of basis functions. In order to define a cost functional adapted to our clustering problem, we need to define a measure of the separation between two clusters of wavelet packet coefficient $\alpha_\gamma(\mathbf{x}_i)$, for a given basis vector ψ_γ. We partition the set of coefficients $\{\alpha_\gamma(\mathbf{x}_i),\ i = 0, \cdots, N - 1\}$ into 2 clusters, and we define $\mu_{i,c}$ to be the membership value of the wavelet packet coefficient $\alpha_\gamma(\mathbf{x}_i)$ in the cluster c. $\mu_{i,c}$ is a real number in $[0, 1]$ that measures the likelihood that $\alpha_\gamma(\mathbf{x}_i)$ belongs to the cluster c, ($\mu_{i,1} + \mu_{i,2} = 1$). We first compute the centroid $\overline{\alpha}_\gamma(c) = \sum_{i=0}^{N-1} \mu_{i,c}\alpha_\gamma(\mathbf{x}_i)$ of the cluster c. We then calculate the in-class variance $s_\gamma^2(c) = \sum_{i=0}^{N-1} \mu_{i,c} \left(\alpha_\gamma(\mathbf{x}_i) - \overline{\alpha}_\gamma(c)\right)^2 /(N - 1)$ of each cluster c. A good separation will be achieved if the distance between the cluster centroids is large relative to the in-class variance of each cluster. For a given wavelet packet ψ_γ, $\gamma = (j, k, l)$, the normalized distance between the two clusters, $\mathcal{D}(\gamma)$, is defined by

$$\mathcal{D}(\gamma) = \frac{|\overline{\alpha}_\gamma(c_1) - \overline{\alpha}_\gamma(c_2)|}{\sqrt{s_\gamma^2(c_1)s_\gamma^2(c_2)}}. \tag{4}$$

Our definition of the normalized variance is similar to the definition of the Fisher linear discriminant. As explained in the previous section, we are interested in finding a basis where a small number of basis functions ψ_γ are capable of clustering the wavelet packets coefficients $\alpha_\gamma(\mathbf{x}_i)$ into two clusters with a large distance $\mathcal{D}(\gamma)$. In other words, we favor a sparse distribution of the distances $\{\mathcal{D}(\gamma)\}_\gamma$. To characterize the sparsity of the distribution we compute its entropy. Given a wavelet packet node (j, k), we define the cost function for the subspace $\boldsymbol{\Psi}_{j,k}$ by

$$\mathcal{M}(\boldsymbol{\Psi}_{j,k}) = -\sum_{l=0}^{2^{J_0-j}-1} \frac{\mathcal{D}^2(j,k,l)}{\|\mathcal{D}(j,k,\cdot)\|^2} \log \frac{\mathcal{D}^2(j,k,l)}{\|\mathcal{D}(j,k,\cdot)\|^2}, \tag{5}$$

where $\|\mathcal{D}(j,k,\cdot)\|^2 = \sum_{l=0}^{2^{J_0-j}-1} \mathcal{D}^2(j,k,l)$. $\mathcal{M}(j,k)$ will be maximum if all the wavelet packets $\boldsymbol{\psi}_{j,k,l}$ at the node (j,k) have the same distance $\mathcal{D}(j,k,l)$. Such a subspace of wavelet packets will be of no interest for our purpose.

3.1   Local Clustering Basis Selection

We are now ready to define the best clustering basis algorithm. This algorithm searches for the optimal basis according to the criterion defined in (5). The wavelet packet tree (see Fig. 2) is explored from the bottom up, and the optimal combination of the $\boldsymbol{\Psi}_{j,k}$ is kept. The search proceeds as follows. Given a set of N time-series vectors $\{\mathbf{x}_i\}_{i=0}^{N-1}$, indexed by their position i,

1. **Wavelet packet expansion**.
   For each vector $\mathbf{x}_i$, compute the wavelet packet coefficients $\alpha_\gamma(\mathbf{x}_i)$ at each node (j,k) of the wavelet packet tree.
2. **Clustering**.
   For each wavelet packet index (j,k,l), cluster the set $\{\alpha_{j,k,l}(\mathbf{x}_i), \ i = 0, \cdots, N-1\}$ into two clusters, and compute the distance $\mathcal{D}(j,k,l)$.
   For each wavelet packet node node (j,k), compute the cost function $\mathcal{M}(\boldsymbol{\Psi}_{j,k})$.
3. **Divide and conquer**.
   For the coarsest scale J, initialize the best basis with $\mathbf{B}_{J,k} = \boldsymbol{\Psi}_{J,k}, k = 0, \dots, 2^J - 1$.
   For the scales $J-1$ until 0, choose the best subspace $\mathbf{B}_{j,k}$ according to

$$\mathbf{B}_{j,k} = \begin{cases} \boldsymbol{\Psi}_{j,k} & \text{if} \quad \mathcal{M}(\boldsymbol{\Psi}_{j,k}) \leq \quad \mathcal{M}(\mathbf{B}_{j+1,2k}) + \mathcal{M}(\mathbf{B}_{j+1,2k+1}) \\ \mathbf{B}_{j+1,2k} \oplus \mathbf{B}_{j+1,2k+1} & \text{otherwise.} \end{cases} \tag{6}$$

The output of the algorithm is the best basis $\mathbf{B}_{0,0} = \{\mathbf{b}_\gamma\}, \gamma \in \Gamma_0$. We have noticed in our experiments that the basis vectors that provide the best clustering power will generate a set of coefficients with a large variance. Because we want to retain only the basis vectors with the largest clustering power, we rank the basis vectors according to their variance $\sigma^2(\gamma)$, and keep the first T_r vectors $\mathbf{b}_{\gamma_l}$ contribute to a percentage r of the total variance. These T_r basis vectors constitute the "clustering" space. The wavelet packet expansion has a complexity of $T \log T$, and the complexity of the search is also $T \log T$.

3.2   Interpretation of the Clusters

If the region W_{i_0} is located in a part of the brain that is activated, then one of the two clusters contains activated voxels, and the other cluster is composed of time

series that describe background activity. According to our experimental findings the cluster with the largest in-class variance $s_\gamma^2(c)$ corresponds to the activated cluster. If the window is in a part of the brain with no activity correlated to the stimulus, then all time series correspond to background activity, and the partition of the time series into two clusters is artificial. In this latter case both the normalized distance $\mathcal{D}_\gamma$ between the two clusters and the total variance of the wavelet packet coefficients are much smaller than when the region W_{i_0} contains a mixture of activated and background time series. We use this observation to discriminate between the two situations : (1) the two clusters come from background activity (unrelated to the stimulus), and (2) one cluster contains the activated time series, and the other the background time series.

4 Experiments

4.1 Synthetic Event-Related Data

We describe in this section experiments conducted on artificial data sets of event-related fMRI time series. The BOLD signal was modeled using the parametric model proposed by Glover [11]. The BOLD signal $y(t)$ is zero before the stimulus onset t_s. If $t > t_s$, $y(t)$ given by

$$y(t) = a_1(t - t_s)^{d_1} e^{-(t-t_s)/t_1} - 0.4 a_2 (t - t_s)^{d_2} e^{-(t-t_s)/t_2} \qquad (7)$$

The normalization constants are given by $a_i = \max((t - t_s)^{d_i} e^{-(t-t_s)/t_i})^{-1}$. We take $t_s = 22.5s$. We consider 32 time samples : $t = [0, 1.5, 3, \dots, 46.5]$. We assume that the parameters of the model are random variables normally distributed: $d_1 \sim N(5, 0.1), d_2 \sim N(12, 0.5), t_1 \sim N(1, 0.2)$, and $t_2 \sim N(0.9, 0.1)$. We have chosen the mean of the random variables to be equal to the values estimated by Glover [11] for a motor response. Fig. 4–**A** shows the mean realization of the event-related signals. We generate four different realizations of $y(t)$ according to (7). We add white Gaussian noise to these time series. The variance of the noise is increased for each experiment. Finally, we generate 16 other time series that are realizations of white Gaussian noise. The ratio of the number of non-activated time series to the number of activated time series is 4 to 1. Six datasets with average SNR=0.1, 0.2, 0.5, 0.8, 1, and 1.5 are generated. We apply the best clustering algorithm and obtain the best clustering basis for each dataset. Fig. 4–**B** shows the first 2 best clustering basis vectors $\mathbf{b}_{\gamma_0}$, and $\mathbf{b}_{\gamma_1}$ obtained with the data with a SNR equal to 0.5. These two vectors capture 40% of the total wavelet packet coefficient variance. These vectors resemble the hemodynamic response function at different delay times and different positive response widths. Fig. 4–**C** shows the scatter plot obtained by projecting a dataset onto the two best clustering basis vectors for SNR = 0.5. The two clusters are well separated. We now compare the performance of our approach with two other standard methods: the t-test [4] and the correlation analysis [12]. The comparison will be based on the number of true and false positives for each value of the SNR. The true activation rate is the ratio between the number of
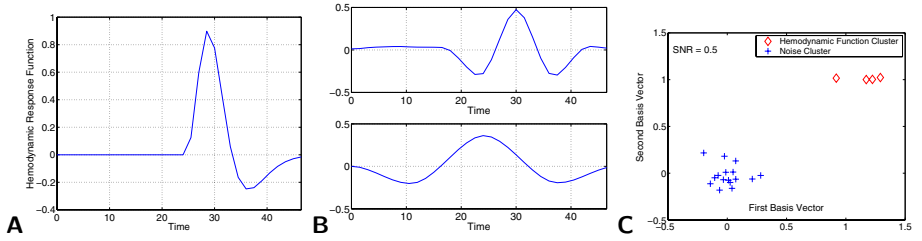
Fig. 4. A : Mean hemodynamic response time series defined by (7). **B** : the best two basis vectors obtained with an SNR=0.5. **C** : scatter plot obtained by projecting all the time series onto the first two best clustering basis vectors.

true positives detected by the algorithm and the total number of true positives. The false activation rate is the ratio between the number of false positives detected by the algorithm and the total number of true negatives. For each value of the SNR, we generate 10 independent datasets. We analyze each dataset, and compute the average true and false activation rates. We describe in the following the details of each method of analysis.

Best clustering basis algorithm. We apply the best clustering algorithm to the data and obtain the reduced feature space by retaining the first T_r vectors $\mathbf{b}_{\gamma l}$ that capture $r = 40\%$ of the total variance of the wavelet packet coefficients. We then project the time series onto this reduced subspace. Finally, we use the fuzzy C-means clustering algorithm to cluster the projected data into two clusters. The cluster c_a with the centroid with the higher energy will be assigned to be the activated cluster. The membership value μ_{i,c_a} measures the likelihood that the time series $\mathbf{x}_i$ is activated. An activation map can be obtained by thresholding μ_{i,c_a}. In our experiments, we use a threshold equal to 0.8.

T**-test.** The t-test assumes that each fMRI time series corresponds to the realization of an identically independent stochastic process and divides the data into two groups, obtained during on (post-stimulus) and off (pre-stimulus) periods. We calculate a t statistic by computing the difference of the sample means of each group normalized by the pooled standard deviation [4]. We then threshold the p-value map at $p = 0.05$.

Correlation analysis (gold standard). We compute the correlation between the time series and the model (7) using the mean values of the random parameters : $d_1 = 5, d_2 = 12, t_1 = 1$, and $t_2 = 0.9$. The correlation threshold is 0.5. We note that the correlation analysis has the perfect knowledge of the (average) true fMRI signal. Because this method represents an ideal situation that cannot be implemented in practice, it provides a challenging gold standard for our algorithm. Fig. 5 shows the average true and false activation rates as a function of the SNR. As expected, the best performance is obtained with the correlation analysis. When the SNR becomes greater than 0.4, the performance of our approach is comparable to the correlation analysis without requiring any knowledge about the hemodynamic response. Indeed, as shown in Fig. 4–right, our
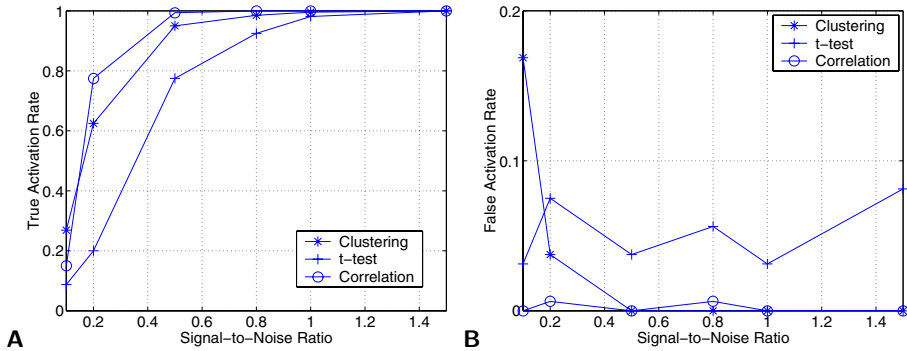
Fig. 5. True activation rate (left) and false activation rate (right) obtained with the best clustering basis algorithm (*), the *t*-test (+), and the correlation method (o).

method can discover automatically the relevant structure of the hemodynamic response. Both the correlation analysis and the best clustering basis algorithm outperform the *t*-test by achieving a higher true activation rate and a lower false activation rate.

4.2   *In-Vivo* **Event-Related fMRI Data**

We present here the results of experiments conducted with event-related fMRI data. The data, provided by Dr. Gregory McCarthy (Brain Imaging and Analysis Center, Duke University), demonstrate prefrontal cortex activation in the presence of infrequent events [13]. Visual stimuli were presented to the subjects: most of the images were squares. Infrequent events (targets) consisted in the appearance of circles at random time. A picture was displayed every 1.5 seconds. The subject was asked to mentally count the number of occurrences of the circles and report that number at the end of each run for a total of 10 runs. The experiment was designed to study whether the processes that elicit P300, an event-related potential caused by infrequent target events whose amplitude is dependent on the preceding sequence of stimuli, could also be measured by fMRI [13]. The data was acquired with a gradient echoplanar EPI sequence (TR = 1500 ms, TE = 45 ms, NEX = 1, FOV = 40 × 20 cm, slice thickness = 7 mm, and imaging matrix 128 × 64). More details about the experiments are available in [13]. We extract 16-image segments consisting of the 8 images preceding and the 8 images following each target. We have in each run about 5 to 6 targets for a total of about 52 targets. We average the 52 segments in order to increase the SNR. This average signal constitutes the time series $\mathbf{x}_i$. We correct for baseline differences by subtracting from $\mathbf{x}_i$ the pre-stimulus mean value. We place a 4 × 4 window W_{i_0} into two different regions: (A) a region where we expect to see activation, and (B) a region where we expect no activation (see Fig. 6–**A**). For each position we compute the best clustering basis based on the 16 time series inside the window. Fig. 6–**B** shows the first two basis vectors ($\gamma = (1, 0, 1)$, and $(1, 0, 2)$)
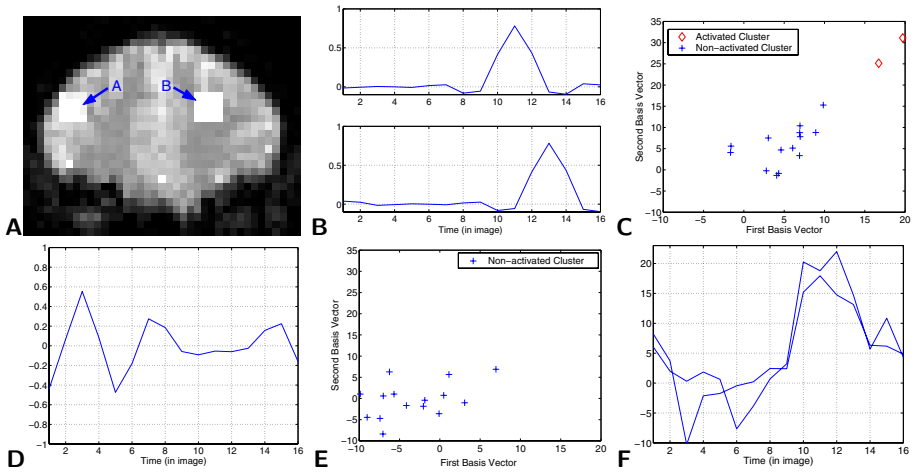
Fig. 6. A : Two 4×4 windows are placed in a region (A) where we expect activation, and in (B) where we expect no response related to the stimulus. **B** : two most discriminating basis vectors ($\gamma = (1, 0, 1), (1, 0, 2)$) for region (A). **C** : Scatter plot obtained by projecting the fMRI time series from region A onto the first and the second basis vectors. The class membership is determined using the fuzzy C-mean clustering algorithm with the membership value threshold of 0.8. **D** : most discriminating basis vector for region (B). **E** :Scatter plot obtained by projecting the fMRI time series from region (B) onto the first and the second basis vectors. **F** : time series extracted from the two voxels detected as activated by both the best clustering algorithm and the t-test.

that capture 40% of the total variance for region A. We note that these two vectors, that were discovered automatically by the algorithm, behave as some delayed hemodynamic responses. Figure 6–**D** shows the first best basis vector for region B. This function has no specific features. A scatter plot obtained by projecting the 16 time series on the two best clustering vectors is shown for each region A and B in Fig. 6–**C** and **E**. As expected, the scatter plot of the region with no activation (B) is fairly compact, whereas the scatter plot of region A is elongated and shows two well defined clusters. We confirm this visual impression by measuring the distance between the cluster centroids for both regions. Obviously, the clusters in region B are not meaningful but the distance between the centroids provides a quantitative measurement of the spread of the coefficients. The distance between the centroid is 2.01 for region A and 0.9 for region B. The total variance of the wavelet packets coefficients is 55 for region A and 20.5 for region B. This clearly demonstrates that both the distance between the cluster centroids as well as the total variance within the window W_{i_0} can be used to discriminate between activated and non-activated regions. The activated time series $\mathbf{x}_i$ were detected by thresholding the membership value μ_{i,c_a} at a level of 0.8. For comparison purposes, we also computed an activation map using the t-test. The p-value threshold was 0.005. The two activation maps shown in Fig. 7 are identical. The two time series detected as activated by the clustering algo-
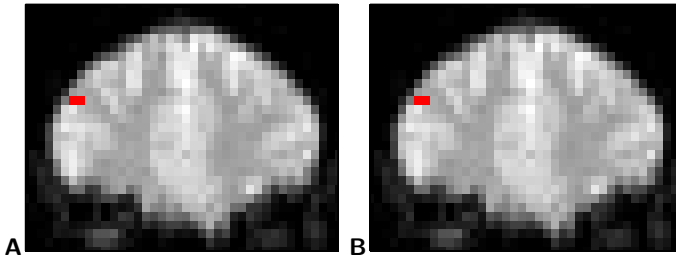
Fig. 7. Left: Activation map obtained by clustering wavelet packet coefficients of the two basis vectors. The membership value threshold is 0.8. Right: activation map obtained using the t-test with p-value threshold $= 0.005$.

rithm and by the t-test are shown in Fig. 6–**F**. They have the shape expected for hemodynamic responses. We also notice that the two best clustering vectors shown in Fig. 6–**B** perform as matched filters to detect these time series.

5   Conclusion

We have presented an algorithm that constructs a clustering basis that best separates activated time series from background noise using a small number of basis functions. Unlike most fMRI data analysis methods our approach does not require any model of the hemodynamic response or any *a priori* information. We have shown with several experiments conducted on synthetic data that our approach was capable of finding the basis that best concentrated its discriminatory power on the fewest number of its vectors. The projection of the original data on the first few basis vectors always revealed the organization of the data. We also applied our method to an *in-vivo* event-related fMRI dataset. The best clustering basis included a small number of vectors that had the characteristic features of an hemodynamic response. We have also shown that when the spatial window is placed inside a non-activated region, the best basis could not separate the time series into meaningful clusters. In this case, the basis functions resembled noise and did not possess any relevant structures. We have assumed in all the synthetic experiments that the noise was white and Gaussian. This is clearly not the case for experimental fMRI data. It has been noticed by several authors that data collected under the null-hypothesis condition exhibit the $1/f$ spectrum associated with long memory processes [14, 15]. The colored noise can be uncorrelated by the wavelet transform. It has been shown [16] that the wavelet transform approximates the Karhunen-Loève transform for processes with $1/f$ spectrum. We can therefore assume that the noise in the wavelet domain is uncorrelated and Gaussian.

References

1. Magnus, K., Nichols, T., Poline, J.B., Holmes, A.: Statistical limitations in functional neuroimaging ii. signal detection and statistical inference. Phil. Trans. R. Soc. Lond. B (1999) 1261–81
2. Vazquez, A., Noll, D.: Nonlinear aspects of the BOLD response in functional MRI. Human Brain Mapping **7** (1998) 108–118
3. Golay, X., Kollias, S., Stoll, G., Meier, D., Valavanis, A., Boesiger, P.: A new correlation-based fuzzy logic clustering algorithm for fMRI. Magnetic Resonance in Medicine **40** (1998) 249–260
4. Lange, N., Zeger, S.: Non-linear Fourier time series analysis for human brain mapping by functional magnetic resonance imaging. Appl. Statist. **46** (1997) 1–29
5. Mitra, P., Pesaran, B.: Analysis of dynamic brain imaging data. Biophysical Journal **76** (1999) 691–708
6. Bullmore, E., Long, C., Suckling, J., Fadili, J., Calvert, G., Zelaya, F., Carpenter, T., Brammer, M.: Colored noise and computational inference in neurophysiological (fMRI) time series analysis : resampling methods in time and wavelet domain. Human Brain Mapping **78** (2001) 61–78
7. Raz, J., Dickerson, L., Turetsky, B.: A wavelet packet model of evoked potentials. Brain Lang **66:1** (1999) 61–88
8. Coifman, R., Wickerhauser, M.: Entropy-based algorithms for best basis selection. IEEE Trans. Information Theory **38** (1992) 713–718
9. Mallat, S.: A Wavelet Tour of Signal Processing. Academic Press (1999)
10. Saito, N.: Classification of geophysical acoustic waveforms using time-frequency atoms. Proc. Am. Statist. Assoc. Statist. Computing (1996) 322–7
11. Glover, G.: Deconvolution of impulse response in event-related bold fMRI. NeuroImage (1999) 416–429
12. Friston, K., Jezzard, P., Turner, R.: Analysis of functional MRI time-series. Human Brain Mapping **1** (1994) 153–171
13. McCarthy, G., Luby, M., Gore, J., Goldman-Rakic, P.: Infrequent events transiently activate human prefrontal and parietal cortex as measured by functional MRI. Journal of Neurophysiology **77** (1997) 1630–4
14. Zarahn, E., Aguire, G., D'Esposito, M.: Empirical analysis of BOLD fMRI statistics : I. Spatially unsmoothed data collected under null hypothesis conditons. Neuroimage **5** (1997) 179–197
15. Fadili, J., Bullmore, E.: Wavelet-generalized least squares : a new BLU estimator of linear regression models with $1/f$ errors. NeuroImage **15** (2002) 217–232
16. Wornell, G.: A Karhunen-Loève-like expansion for $1/f$ processes via wavelets. IEEE Trans. on Info. Theory **36** (1998) 859–61